2627

NRL Report 7285

Bistatic Acoustic Scattering From the Ocean Bottom

B. G. Hurdle, K. D. Flowers, and K. P. Thompson

Propagation Branch
Acoustic Division

August 5, 1971

AD 0728745

NAVAL RESEARCH LABORATORY
Washington, D.C.

Approved for public release; distribution unlimited. DDC-A

CONTENTS

Abstract	ii
Problem Status	ii
Authorization	ii
INTRODUCTION	1
DATA ANALYSIS	1
Scattering Strength	1
Effect of Gradients	3
Working Equations	3
THE EXPERIMENT	4
Instrumentation	4
Geometry	4
Operating Area	4
Results	4
THE SCATTERED ACOUSTIC FIELD	5
Discussion	5
Attenuation in the Bottom	10
Percentage of Power Scattered	10
SUMMARY AND CONCLUSIONS	11
REFERENCES	11
APPENDIX A — Refraction and Absorption	13
APPENDIX B — Instrumentation and Procedures	15

ABSTRACT

To obtain the intensity field of sound scattered from a relatively rough region of the ocean bottom, pulsed 19.5-kHz transmissions were directed toward the bottom from a ship as it approached and passed a special radio sonobuoy. Sets of data were taken with the beam incident on the bottom at grazing angles between 30 and 90 degrees. Bottom scatter returns in the monostatic direction were received on the source transducer, while reception in other directions was made by the buoy. The source was a tiltable piston transducer with a beamwidth of approximately 8 degrees. The buoy hydrophone was omnidirectional in the horizontal plane with a rejection of surface-reflected signals in the vertical plane. The data were analyzed on the basis of an isotropic-scatter model, taking the velocity gradient into consideration. Polar plots were made of bottom scattering strength. These intensity fields have been obtained from areas east of Bermuda for two bottom types, mud-coral and ooze, in water depths of approximately 750 and 1250 fathoms respectively. The results were compared with geometric reflection and Lambert's scattering law and did not correspond with either or with a combination of both. The shape of the plots of the measured field, combined with data indicating significant acoustic penetration into the bottom and data on the quantity of energy penetrating, suggests that a significant contribution to the field is made by a transmission path through the bottom. Sediment attenuation data in this frequency range, however, are inconclusive as to whether a significant contribution by refraction paths through the bottom exists.

Problem Status

This is an interim report on the NRL Problems: work is continuing.

AUTHORIZATION

NRL Problems S01-12 and S01-40
Projects RF 101-03-44-4059, RF 05-552-402-Task 4070
and SF 101-03-15-8181

Manuscript submitted April 7, 1971.

BISTATIC ACOUSTIC SCATTERING FROM THE OCEAN BOTTOM

INTRODUCTION

Reflection and scattering in the ocean have always been a major source of interference in the operation of underwater sound equipment. Now that higher powered and more directive low-frequency sources make possible the increase of signal levels relative to the ambient noise background, the interference caused by reflection and scattering, commonly referred to as reverberation, may become the predominant interference in underwater sound applications.

Underwater sound technology now makes feasible the transmission of sonar information over new paths, many of which intercept the bottom or surface or both. Therefore, to understand the nature and predict the performance of acoustic signals traveling over these paths, we must know the physical mechanisms of reflection and scattering. Specifically, we need to know how the reflected and scattered acoustic field behaves for a large variation in oceanographic conditions and why it behaves this way. Not only do we need to know how the energy is distributed, but what transformation or degradation a signal will undergo when transmitted via a boundary.

This report will be confined to reflection and scattering from the ocean bottom. Many authors have dealt with scattering from the ocean bottom in the backward or monostatic case, in which the receiver is located at the point of transmission. This case has also been given extensive treatment in the scattering of electromagnetic energy from various boundaries such as the sea surface, various types of terrain, and the ionosphere.

Investigations of reflection and scattering from the ocean bottom in directions other than the monostatic case are confined mostly to the region near the specular direction. The BRASS II project has made measurements of bottom loss in and near the specular direction over a limited range of grazing angles.

Urick [1] made a set of measurements in shallow water at 22 kHz, employing a geometry (Fig.1) in which the sound was incident on the bottom at grazing angles θ less than 1° with reception over a range of azimuth angles ξ from 30° to 180°, at the same 1° elevation angle ψ. He concluded that the field, for the region investigated, was scattered isotropically.

Nolle et al. [2] conducted laboratory experiments in a tank on the scattering of sound from water-filled sand surfaces. The shape of the scattered intensity field was obtained in terms of the scattering coefficient for the sound impinging on the bottom at grazing angles θ of 45°, 70°, and 90°. The acoustic field obtained in these measurements is characterized by a large reflected peak in the specular direction $\psi = \theta$, $\xi = 0°$ and a broad plateau of scattered intensity that decreases as the two scatter angles $\psi = 0°$, $\xi = 0°$ and 180° are approached. These data indicate a simple combination of specular reflection and Lambert's law scattering.

DATA ANALYSIS

Scattering Strength

The measured data must be considerably reduced for a meaningful presentation of the scattered acoustic field. The approach chosen here is similar to that used in displaying

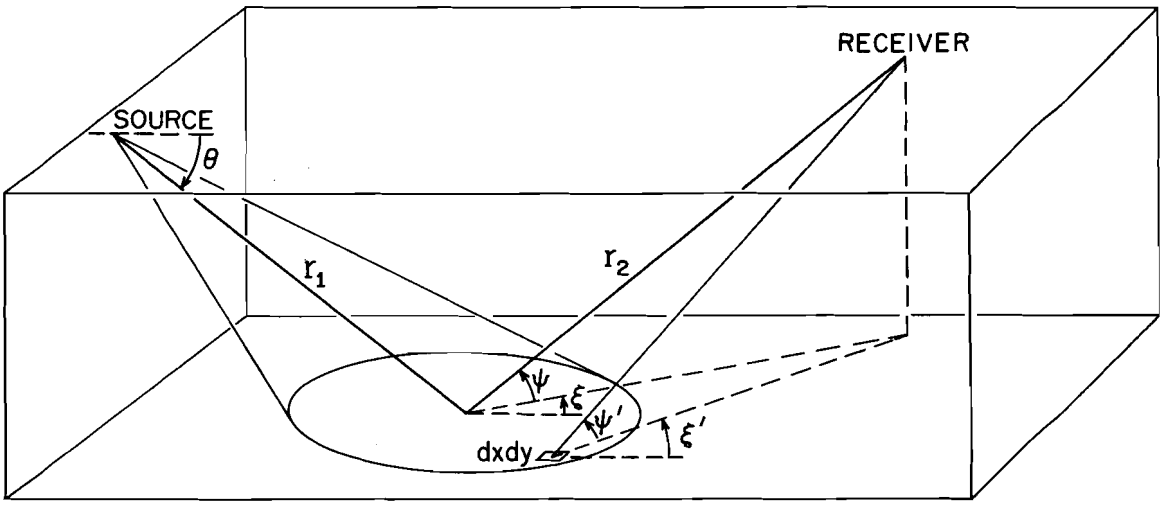

Fig. 1 - Scattering geometry

the field of an acoustic source, in which the intensity is plotted radially versus the angle, with the center of the radiator at the pole.

The scattering strength, a common criterion describing a scattering characteristic of a boundary, is used in this analysis, being displayed as a function of the geometry. Scattering strength is based on the isotropic scatter model of Eckart [3] except, following Urick [1], the scattering strength is used rather than the scattering coefficient. Scattering strength s is defined as

$$s = \frac{I_s}{I_i A} \, yd^{-2}, \tag{1}$$

where I_s is the scattered intensity, referred to 1 yard from the center of the ensonified area on the bottom, in the direction of observation (dyne sec^{-1} cm^{-2}), I_i is the intensity incident on the bottom (dyne sec^{-1} cm^{-2}), and A is the area of ensonification on the bottom (yd^2).

For the present case the incident intensity was not a constant over the ensonified area due to the directivity of the source. This necessitates a reformulation of the above; for fixed depression angle θ

$$I_s(\Psi, \xi) = \iint_A s(x, y; \Psi', \xi') \, I_i(x, y) \, dxdy,$$

where (Fig. 1) Ψ and ξ are respectively the elevation and azimuth angles of the receiver with respect to the center of the ensonified area and Ψ' and ξ' are respectively the elevation and azimuthal angles of the receiver with respect to $dxdy$.

We assume that s can be considered a constant for the small beamwidth used; that is, $|s(x, y, \Psi', \xi') - s(\Psi, \xi)|$, $|\Psi' - \Psi|$, and $|\xi' - \xi|$ are all small for $(x, y) \in A$. Then

$$I_s(\Psi, \xi) = s(\Psi, \xi) \iint_A I_i(x, y) \, dxdy$$

or

$$s(\Psi, \xi) = I_s(\Psi, \xi) \left[\iint_A I_i(x, y) \, dxdy \right]^{-1}. \tag{2}$$

Since the intensities incident on and scattered from the bottom are by definition those on and 1 yard from the effective center of the scattering area respectively, the data measured at the surface must be referred to these points. For a directive source with substantially all of the energy contained in the main beam the double integral in Eq. (2) represents the total power impinging on the bottom. Thus attenuation is the only loss to account for on the downward path. The scattered intensities at the receiver are referred to a point 1 yard from the bottom. This requires accounting for both spreading and attenuation losses over the path from the bottom to the receiver.

Effect of Gradients

Most measurements of acoustic propagation in the ocean are subject to the anisotropic effects of temperature, pressure, and salinity gradients. This experiment was no exception, and significant effects of these gradients were taken into account.

Since all distances were determined from the measurement of acoustic transit time, the average sound speed of propagation over the path through the sound-speed gradient was required. The second effect of the sound-speed gradient accounted for was refraction, which provided the correct geometry. The third effect, associated with the intensity, provided the correct spreading loss, since the sound-speed gradient causes it to deviate from square law. The last effect of the sound-speed gradient accounted for was the average absorption over the path. Each of these effects are discussed in more detail in Appendix A.

Working Equations

From Eq. (2)

$$S(\Psi, \xi) = 10 \log s(\Psi, \xi) = 10 \log [I_s(\Psi, \xi)] - 10 \log \left[\iint_A I_i(x, y)\, dxdy \right]$$

When propagation is included,

$$10 \log [I_s(\Psi, \xi)] = E - M - G + 20 \log r_2 + Kr_2 + B$$

and

$$10 \log [\iint_A I_i(x, y)\, dxdy] = L + 20 \log i - D - Kr_1 + 10 \log \left[\iint_A b(x, y)\, dxdy \right],$$

so that

$$S = E - M - G + 20 \log r_2 + K(r_1 + r_2) + B - L - 20 \log i + D - 10 \log \left[\iint_A b(x, y)\, dxdy \right],$$

where

E = 20 log (scattered-signal amplitude at the receiver),

M = receiving sensitivity,

G = receiver gain,

B = buoy beam-pattern correction,

L = transmitting response,

i = source current,

K = average absorption coefficient,

D = dome loss,

$b(x, y)$ = normalized source radiation function,

r_1 = path length from the source to the scattering area,

r_2 = path length from the scattering area to the receiver.

Any self-consistent set of units may be used for these quantities.

When the signal was received on the same unit as used in transmitting (monostatic case), the preceding quantities are the same except $B \rightarrow D$, $r_2 \rightarrow r_1$, and $b(x, y) \rightarrow [b(x, y)]^2$. For the particular source used in this experiment, numerical evaluation gave

$$10 \log \left[\iint_A b(x, y)\, dxdy \right] = -16.7 \text{ dB}$$

and

$$10 \log \left[\iint_A b^2(x, y)\, dxdy \right] = -19.1 \text{ dB.}$$

THE EXPERIMENT

Instrumentation

The instrumentation and procedures for conducting this experiment are discussed in Appendix B.

Geometry

Data for obtaining the shape of the scatter field were acquired by using a directive source mounted in the USS Rockville (EPCER 851) and a buoy-supported hydrophone with a radio link to the ship. Acoustic pulses were transmitted to the bottom at a depression angle θ. Signals scattered from the elliptical area on the bottom were received at the buoy hydrophone and at the source transducer.

The source ship was maneuvered to traverse past the buoy, thus continuously varying Ψ and ξ, the bottom scatter angles. This enabled a series of scatter angles to be obtained for each of several tilt angles of the source.

Operating Area

The experiment was conducted on the east slope of the Bermuda Rise over areas 1, 2, and 3 indicated in Fig. 2. Areas 1 and 3 have a bottom characterized by the Naval Oceanographic Office as mud-coral. A majority of the data were obtained in area 1, which had an average water depth of 750 fathoms. Area 3 has the same characteristics as area 1, except for steeper bottom slopes. Area 2 has an ooze bottom and an average water depth of 1250 fathoms.

Results

The only results presented in this report are for an in-line geometry: $\xi = 0$ or $180°$. Polar plots are presented of the mean scattering strength as a function of Ψ. Data obtained in area 1 are presented in Figs. 3, data obtained in area 2 are presented in Figs. 4, and data obtained in area 3 are presented in Fig. 5. Since in a bistatic

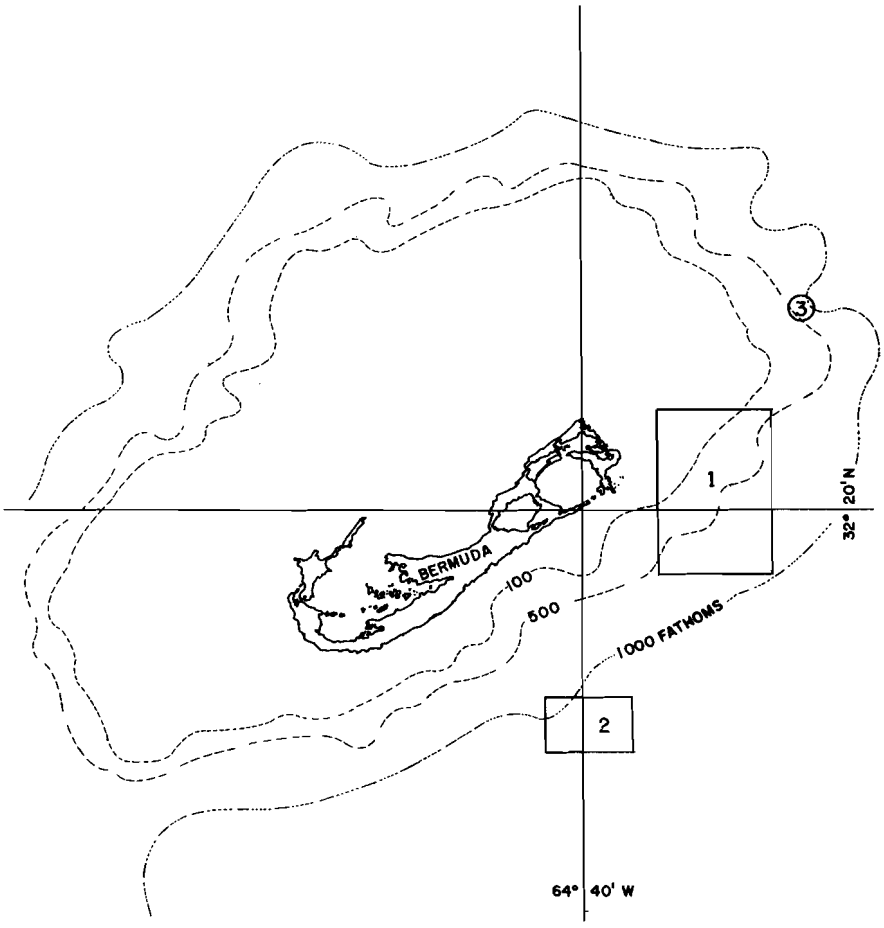

Fig. 2 - Operating areas

experiment of this type complete coverage of the field is difficult, the data points are averages over 10° increments of Ψ and are averages of varying numbers of data points. The error bars at each point indicate ±1 L. S. D. (logarithmic standard deviation), where

$$\text{L.S.D.} \triangleq 10 \log \left(1 + \frac{\sigma}{m}\right),$$

in which σ is the sample standard deviation and m is the sample mean.

THE SCATTERED ACOUSTIC FIELD

Discussion

At first glance the form of the measured acoustic fields suggests a combination of reflection and diffuse scattering (Lambert's law). When these models are applied, however, they are not consistent as the angle of incidence is changed. That is, the "reflection" component is not in the specular direction and deviates from specular by differing amounts depending on the angle of incidence. Also, the "diffuse scattering" component requires a "constant" multiplier which is a function of the incident angle. It is concluded that the scattered fields are not explained by a combination of reflection and diffuse scattering.

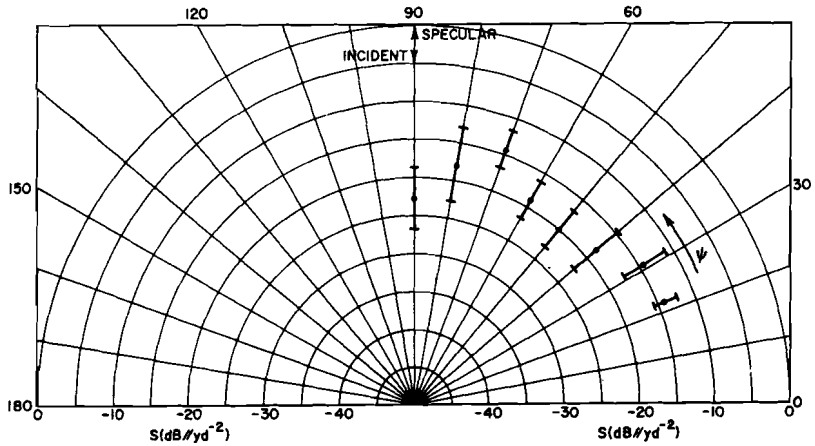

Fig. 3a - Scattering strength S for a depression angle of 90° in operating area 1 (mud-coral bottom)

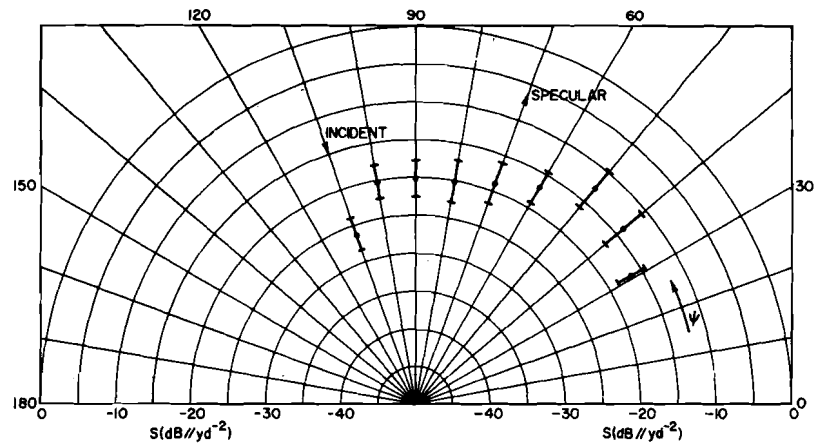

Fig. 3b - Scattering strength S for a depression angle of 70° in operating area 1 (mud-coral bottom)

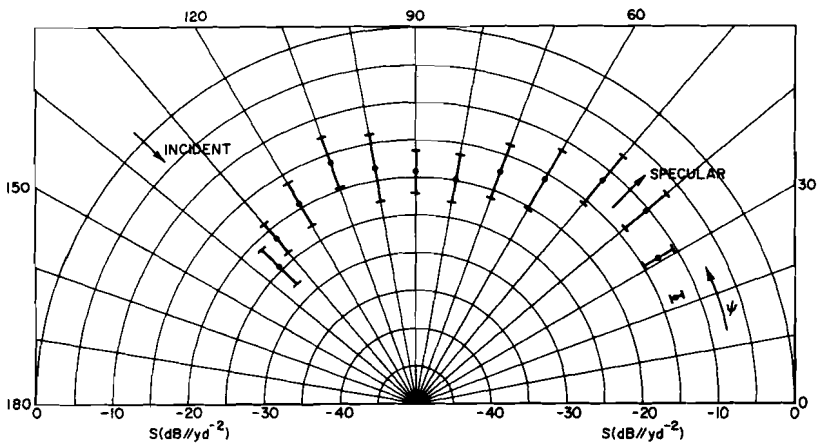

Fig. 3c - Scattering strength S for a depression angle of 45° in operating area 1 (mud-coral bottom)

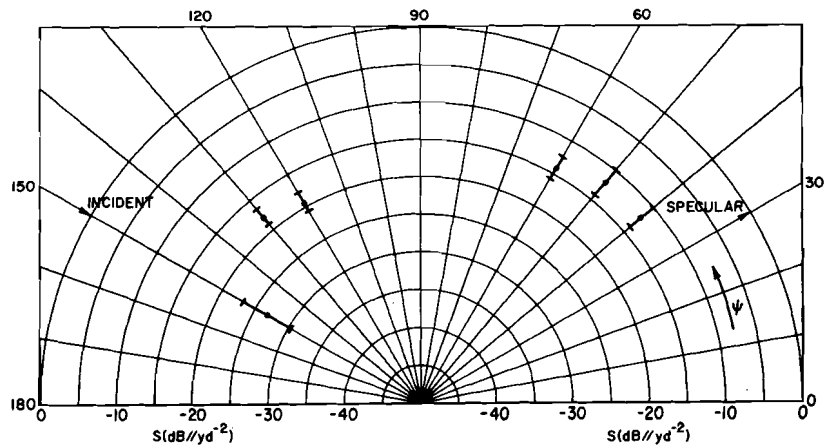

Fig. 3d - Scattering strength S for a depression angle of 30° in operating area 1 (mud-coral bottom)

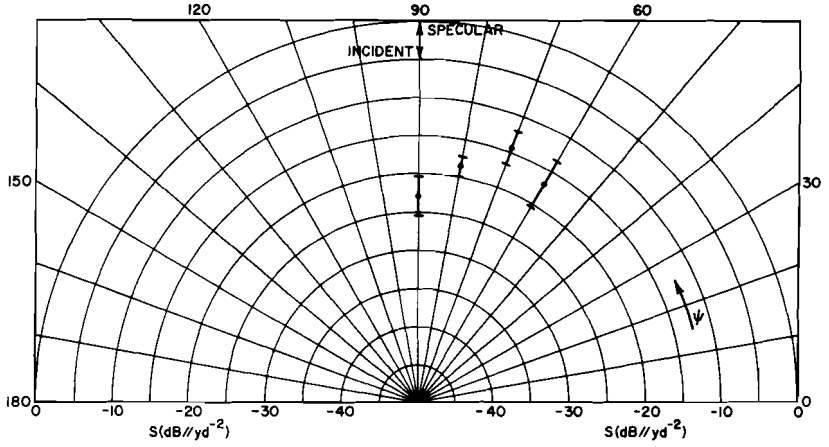

Fig. 4a - Scattering strength S for a depression angle of 90° in operating area 2 (ooze bottom)

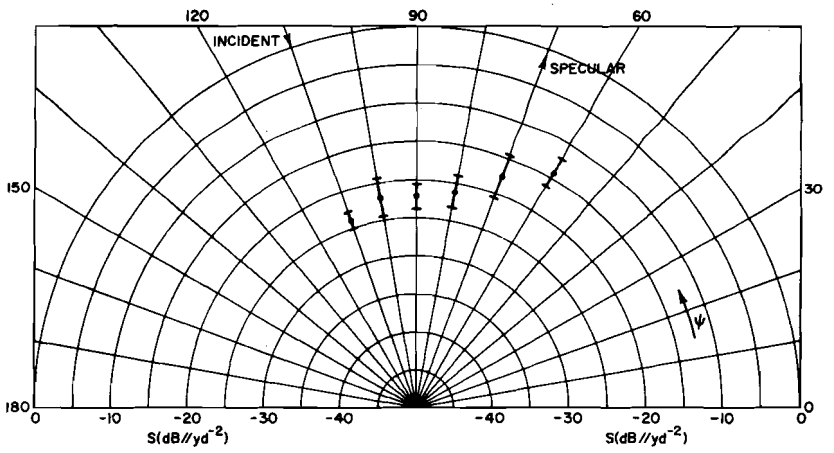

Fig. 4b - Scattering strength S for a depression angle of 70° in operating area 2 (ooze bottom)

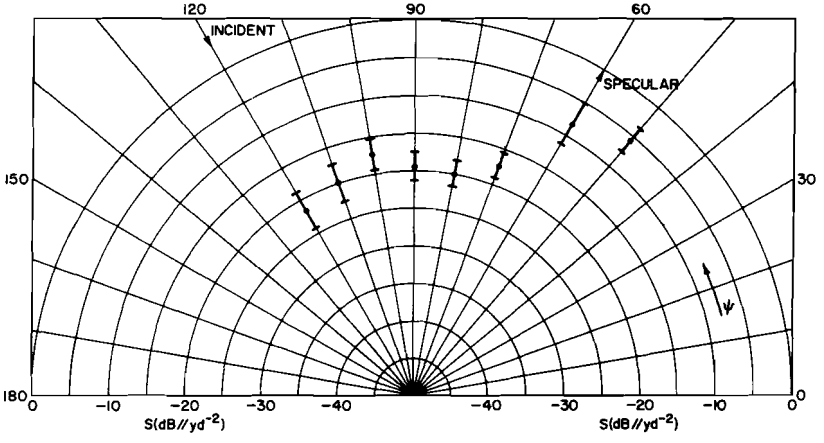

Fig. 4c - Scattering strength S for a depression angle of 60° in operating area 2 (ooze bottom)

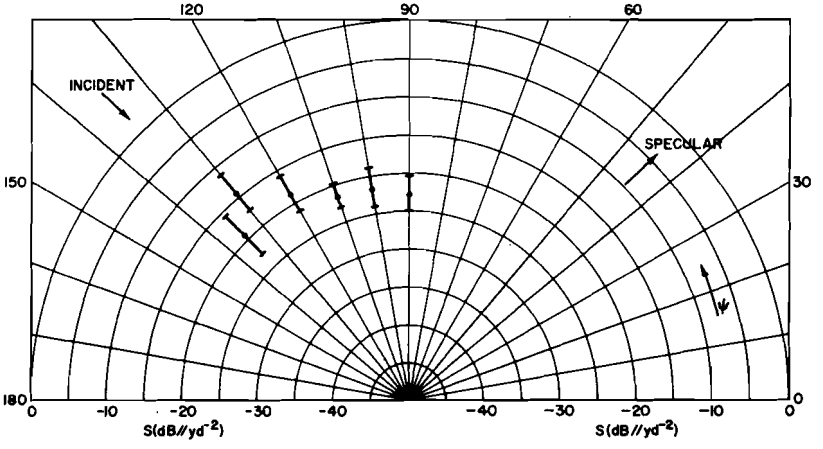

Fig. 4d - Scattering strength S for a depression angle of 45° in operating area 2 (ooze bottom)

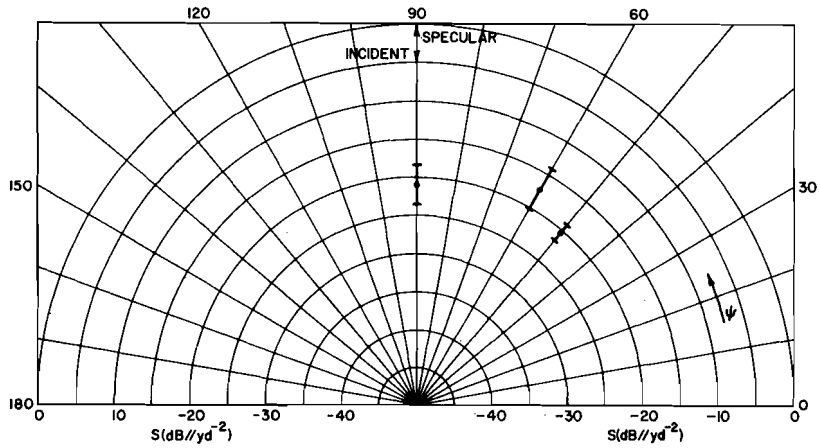

Fig. 5 - Scattering strength S for a depression angle of 90° in operating area 3 (mud-coral bottom)

In addition the individual scattered pulses were extended in time much more than was expected from geometrical considerations.

The operation areas were in general undulating with occasional slopes as high as 20°. Obviously a different average bottom slope for each set of data would explain some of the above discrepancies. However, an average bottom slope large enough to explain the difference between the specular direction and the observed maximum is highly unlikely. Also, the average slopes necessary to explain the reflection component still require a nonconstant multiplier for the diffuse component. Finally the maximum slope (≈20°) encountered does not geometrically extend a pulse sufficiently to explain the observed extension in time. For these reasons it is felt that average bottom slopes do not explain the observed data, although the effect of bottom slope is present in the data to some extent.

Other possible explanations are a subbottom layer or a refraction path through the bottom. The subbottom layer would have to be too far below the bottom to be feasible. The refractive path through the bottom is, ignoring attenuation, capable of explaining the displaced peaks in the results. With the multiple scatter paths associated with this type of bottom the other discrepancies can be expected.

By use of equations found in Horton [4] and the known gradient in the water column the gradient in the bottom necessary to refract the center ray such that it arrived at the surface at the apparent angle of maximum scatter was calculated for Figs. 3b and 4b. These were chosen because the direction of maximum scattering strength is better defined. The calculated gradients were 10.2 and 11.0 sec^{-1} respectively.

A gradient with a magnitude of 10.2 sec^{-1} is considered unusual enough to question its probability of occurrence in this region. Although there are no independent data for this immediate area, Officer and Ewing [5] reported a layer with a sound speed of 4.51 km sec^{-1} obtained from refraction profiling a little east of this area. The calculated vertex sound speed of approximately 4.5 km sec^{-1}, corresponding to a gradient of 10.2 sec^{-1}, is in agreement with this layer sound speed, indicating the possibility of the existence of the gradient.

Figure 6a is a plot of the computed spreading loss as a function of the depression angle θ for a two-layer model (water and bottom) using a gradient of 10.2 sec^{-1} in the

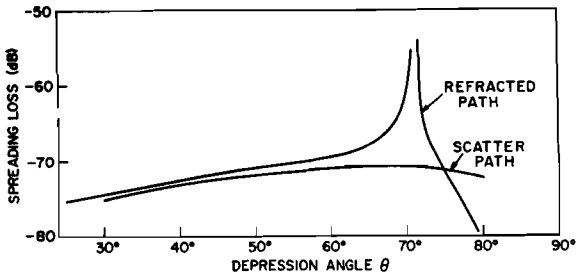

(a) spreading loss to a surface receiver over the refracted path versus the source depression angle as compared to square-law spreading over the scatter path from the layer boundary

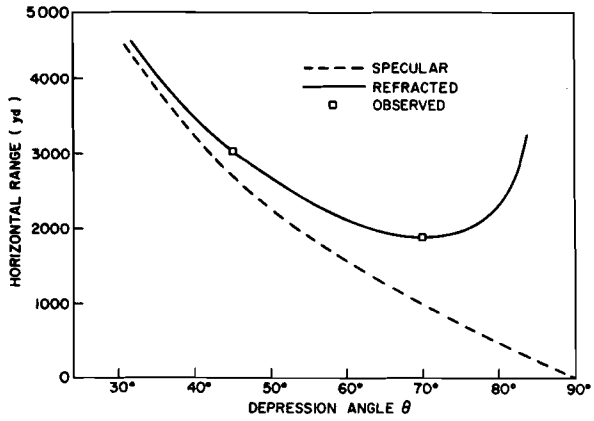

(b) Horizontal range to specular arrival via the refracted path (solid curve) and scatter path (dashed curve) versus the source depression angle

Fig. 6 - Results of an analysis of a two-layer model, water depth of 750 fathoms, water gradient of -0.02, and bottom gradient of +10.2 sec^{-1}

lower layer. For $\theta \approx 70°$ the curve indicates the possibility of a substantial gain over square-law spreading, which is indicated by the line labeled scatter path; square-law spreading is computed to the point where the refracted ray reaches the surface.

Figure 6b is a plot of horizontal range versus the depression angle θ. The dashed curve represents the computed horizontal range from the source to the arrival point of a ray at the surface if specular reflection from the bottom interface was the predominant contributor. The solid curve is the corresponding computed range for rays traversing a refractive path. The two points are from the experimental data, representing the peaks of the 70° and 45° mud-coral patterns. The fit of the experimental points to the refractive curve is superior to a fit to the curve based on specular reflection. The other scatter patterns are not complete enough to give a clear indication of where the peak in the pattern occurs; hence only two experimental points are plotted in this figure. The other patterns do indicate that the points would be above the "specular" curve.

Attenuation in the Bottom

Although a number of factors support a refractive transmission path through the bottom, probably the most important characteristic of the bottom—the acoustic attenuation near 20 kHz—has as yet not been shown to be sufficiently low to make such a path possible.

The material expected in the bottom may be divided into two classes: unconsolidated and consolidated material. Attenuation measurements for a number of unconsolidated sediments have been reported by Shumway [6]. Generally his values range between 0.5 and 10 dB per foot near 20 kHz. If the effective attenuation in the areas investigated here were as much as 0.5 dB per foot, a refractive path through the bottom would be impossible. However, if the unconsolidated sediment existed as a thin layer over consolidated material, the losses over the total refracted path might be sufficiently low to allow it to predominate over the scattered path.

A brief review of the literature concerning losses near 20 kHz in consolidated materials yields a wide range of values. Measurements by Struthers [7] give a range of 0.07 to 0.3 dB per kiloyard for pure fused quartz. These values probably represent a lower limit for this class of material under ideal conditions. The measurements reported by Bergmann [8] also tend to fall in this category. Measurements by Wyllie et al. [9] give an attenuation of 275 dB per kiloyard for marble, and measurements by Born [10] give values of 780 to 1200 dB per kiloyard for sandstone, limestone, and shale. These measurements were made in the laboratory under conditions of atmospheric pressure and no water content.

However, Wyllie et al. [10] also made loss computations, based on a theory of propagation in porous solids by Biot [11,12] of the physical properties of rock structures under conditions of compacting pressure and complete liquid saturation. These computations indicated a substantial reduction of attenuation might be expected with respect to that made under laboratory conditions at atmospheric pressure.

The present authors know of no measurements of the attenuation of sound in deep ocean bottom materials under the conditions of their environment. It has been frequently observed, however, that fathograms in the 12-kHz range show returns from layers much deeper than would be possible if the attenuation was as high as that reported by Shumway [6].

The lengths of the paths required in the bottom are only 0.5 and 0.2 kiloyards respectively for depression angles of 70° and 45°. With Struthers' attenuation values [7] the refractive path would have lower losses than the water path. With reasonable attenuation values (a few tens of decibels per kiloyard) these refractive paths could contribute significantly to the scattered field.

Percentage of Power Scattered

It is of interest to determine the ratio of power returned to the water half-space above the bottom to the power incident on the bottom boundary. This enables one to delineate where the power is dissipated. This power ratio P is obtained by integrating the scatter strength (in power-ratio form) over a hemisphere above the region of scatter.

Inspection of the data indicated that $S(\Psi)$ was symmetrical about the vertical axis of the hemisphere in the normal incidence case or was approximately symmetrical about an axis through the peak* (the cases of 70°, 45°, and 30° incidence) that could be rotated to

*Limited data supporting this thesis were obtained when the ship's heading was not on a line through the source and buoy.

coincide with the vertical axis. This enabled the power ratio to be expressed as

$$P = 2\pi \int_0^{\pi/2} S(\Psi) \cos \Psi \, d\Psi .$$

The integral was evaluated numerically using symmetry arguments and filling in missing data points.

Computations of P, the ratio of power returned to the water to power incident on the bottom, made for the four mud-coral patterns (Figs. 3) are listed below:

Tilt Angle, θ (degrees)	Power Ratio, P
90	0.16
70	0.038
45	0.081
30	0.084

A maximum of approximately 16 percent of the power is returned to the water for the normal incidence case. Thus most of the energy was lost in the bottom, implying good energy transmission into the bottom.

SUMMARY AND CONCLUSIONS

Average scatter fields have been presented in polar plots for various grazing angles. The fields, although not complete, give some idea as to the distribution of energy in the upper half space. They are seen to be complicated and not representable by a combination of reflection and diffuse scattering.

Although much evidence indicates the presence of refraction paths through the bottom, it is not conclusive enough to prove their existence. The biggest argument against them is the attenuation that is usually associated with transmission of 20-kHz sound in reasonable bottom-type materials. If indeed the scatter fields do result from bottom transmission, then the effect must be even larger at lower frequencies.

REFERENCES

1. R.J. Urick, "The Backscattering of Sound from a Harbor Bottom," J. Acoust. Soc. Amer. 26, 231 (1954)

2. A.W. Nolle, W.A. Hoyer, J.F. Mifsud, W.R. Runyan, and M.B. Ward, "Acoustical Properties of Water-Filled Sands," J. Acoust. Soc, Amer. 35, 1394 (1963)

3. C. Eckart, editor, "Principles and Applications of Underwater Sound," NDRC Summary Technical Reports, Division 6, Vol. 7, Washington, D.C. (1946)

4. J.W. Horton, "Fundamentals of Sonar," 2nd edition United States Naval Institute, Annapolis, Maryland, 1959

5. C.B. Officer and M. Ewing, "Seismic Refraction Measurements in the Atlantic Ocean, Part IV, Bermuda, Bermuda Rise, and Nares Basin," Bulletin of the Geological Society of America 63, 779-809, (1952)

6. G. Shumway, "Sound Speed and Absorption Studies of Marine Sediments by a Resonance Method," Geophysics 25, 451 (1960)

7. F. Struthers, unpublished data from work at NRL on solid quartz rods in a vacuum (1944)

8. L. Bergmann, Table 88, p. 654, Ultrasonics (S. Hirzel Verlag Zurich), 1954

9. M.R.J. Wyllie et al., "Studies of Elastic Wave Attenuation in Porous Media," Geophysics 27, 569 (1962)

10. W.T. Born, "The Attenuation Constant of Earth Materials," Geophysics 6, 132-148 (1941)

11. M.A. Biot, "Theory of Elasticity and Consolidation for a Porous Anisotropic Solid," J. Appl. Phys. 26, 182-185 (1955)

12. M.A. Biot, "Theory of Propagation of Elastic Waves in a Fluid-Saturated Porous Solid," J. Acoust. Soc. Amer. 28, 168-191 (1956)

Appendix A

REFRACTION AND ABSORPTION

The sound-speed profile illustrated in Fig. A1 was constructed from the profile of average temperature versus depth obtained in the operating areas (shown in the same figure), using Mackenzie's* equation as modified by Del Grosso's† constant and assuming a constant salinity of 35°/000.

By dividing the sound-speed profile into linear segments, all the pertinent refraction effects were computed: ray path lengths, associated scattered and reception angles, spreading losses over the scattered path, and average velocities over the ray paths.

With the relation between absorption and temperature known (left-hand curve in Fig. A2) and the relation between temperature and depth known (left-hand curve in Fig. A1), the absorption is then calculated from

$$K = \frac{1}{d} \int_0^d k(z)\, dz,$$

where the effects of pressure and salinity changes on $k(z)$ have been ignored. The resulting profile for K is presented on the upper right of Fig. A2.

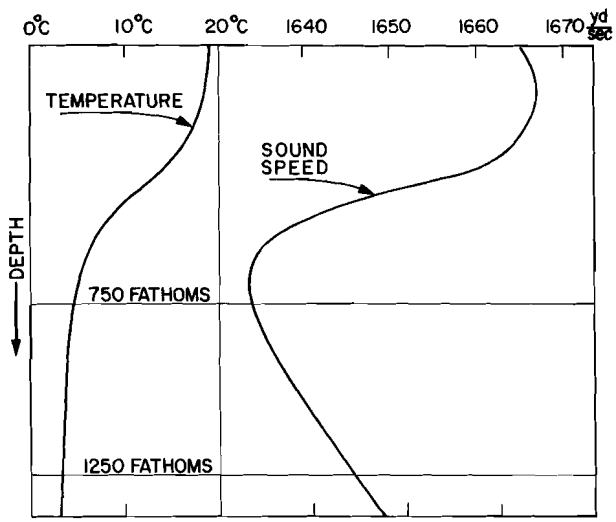

Fig. A1 - Profile of the average measured temperature (left) and profile of the computed average sound speed (right) for the experiment

*K. V. Mackenzie, "Formulas for Computation of Sound Speed in Sea Water," J. Acoust. Soc. Amer. 32, 100 (1960).

†V.A. Del Grosso, NRL Report 4002 (1952) and NRL Report 4279 (1954).

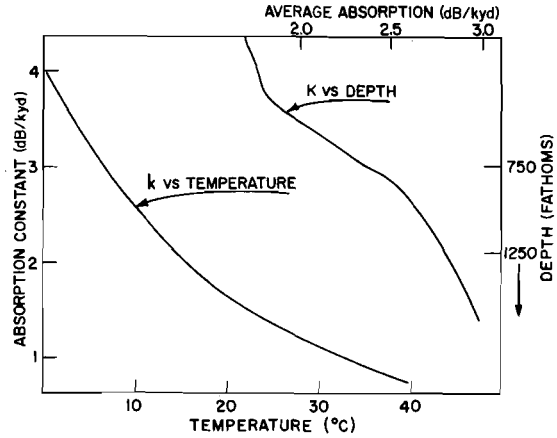

Fig. A2 - Absorption of 20-kHz sound as a function of water temperature (left) and profile of the average absorption over a path to depth d

Appendix B

INSTRUMENTATION AND PROCEDURES

TRANSMITTING

The transmitted signal originated in a crystal-stabilized oscillator that established the 19.5-kHz frequency of the system. The signal passed through a gate circuit actuated by impulses from the timing control unit, which determined the duration of the signal pulses as well as the interval between them. The pulses so formed then went through an attenuator, which set the signal level, into a 1000-watt McIntosh power amplifier. The high-level signal pulses were passed through a series inductive matching network, thus matching the driver to the transducer. A transfer relay, also controlled by the timing control unit, switched the transducer from the receiving circuits to the output of the matching network just prior to the initiation of the signal pulse, maintaining the connection for the duration of the signal pulse.

The source transducer, designated XDV-1, was a plane circular piston type having a directivity index of -27.1 dB at 19.5 kHz. Its main lobe is approximately 8° wide at the half power points with all side lobes down 17 dB or greater. A calibration of all pertinent characteristics was made by the NRL Underwater Sound Reference Division in their USRL Calibration Reports 1535 and 1968.

RECEIVING

The receiving system encompassed those components which received, selected, and amplified the acoustic signals from the water but did not involve the actual recording of data. The following discussion of the receiving system will treat the monostatic system separately from the remote buoy system.

Monostatic Reception

The acoustic energy in the water scattered back from the ensonified area was converted into electrical signals in the XDV-1 transducer used for transmitting. The receiving beam pattern was the same as the transmitting pattern. Signals from the transducer were connected to a constant-gain preamplifier by the normally closed contacts of the transfer relay. As described for the transmitting system, the transfer relay disconnected the transducer from the preamplifier during the transmission. In the normal receiving condition the transducer signals were amplified in the preamplifier and passed through the operate position of the calibrate-operate switch to a decade attenuator, where the system gain was adjusted, before amplification in a tuned, high-gain amplifier, for presentation to the various displays and recording media.

Remote Buoy System

The principal component of the remote buoy system was a special radio sonobuoy, constructed to accommodate a wide range of levels and wave forms of underwater acoustic signals. The hydrophone used was a specially designed unit, suspended approximately 15 feet below the surface. It has a barium titanate cylinder 1-1/2 inches in diameter and

1-1/2 inches long centrally mounted in a 3-inch-diameter pressure release cylinder, with the sound exciting the barium titanate through the central cavity, which was open to the sea at the underside of the transducer. This construction provided a transducer with a sensitivity of approximately 97.8 dB below 1 volt per microbar and a cardioid-type pattern, which effectively suppresses signals reflected from the surface of the ocean. After the signal from the transducer was amplified in the amplifier section of the sonobuoy, it modulated an FM transmitter, broadcasting in the 162-to-174-MHz frequency band. The amplifier-transmitter combination operated linearly over a signal dynamic range of approximately 60 dB, broadcasting at 0.25 watt for approximately 6 hours on a battery load. The radio signal was received aboard ship by a telemetering type FM receiver, tuned to the sonobuoy frequency. The output of the FM receiver passed through the operate position of the calibrate-operate switch and thence through a decade attenuator, in which the system gain was set. It was then amplified in a tuned, high-gain amplifier for presentation to the various displays and recording media.

MEASUREMENT SYSTEM

The measurement system included all components for displaying, recording, and measuring the outputs of the two receiving systems. The signals underwent demodulation and logarithmic amplification for simultaneous recording on the two channels of a Brush two-channel ink recorder. The signals were also displayed on the two beams of a dual-beam cathode-ray oscillograph. A strip film camera that was focused on the cathode-ray tube was available to provide additional recording. The camera was provided with a control unit that intermittently started and stopped the film travel, to conserve film during the time between receipt of the echo and initiation of the next outgoing transmitted pulse. In addition a serial time-code generator, which provided sequentially coded values of the time in minutes and seconds, updated every second, provided by way of an argon glow lamp flasher in the camera a record of time along the edge of the strip camera film. This was used for time correlation of the film record with other data.

A single-beam cathode-ray oscilloscope was used in addition to the dual-beam oscilloscope for visually monitoring the signal from the remote buoy system. A display of a range mark by momentary z-axis brightening of the scope trace assisted in the primary function of this display, which was to facilitate system gain settings and calibrations as well as acoustically tracking the buoy in range and bearing, or tracking the bottom ensonified area in tilt.

The location of the buoy had to be known to accurately establish the geometry of the ship-bottom-buoy system. Although the buoy was accurately tracked in bearing by optical means, range had to be determined by measurement of transit time of the direct transmission of sound from the ship-mounted transducer to the buoy hydrophone. Although the direct path is off the main lobe of the ship-mounted transducer, sufficient energy arrived at the buoy hydrophone to provide a good signal for ship-to-buoy range measurement. This direct signal was fed to the stop channel of a time-interval meter whose timing cycle was initiated simultaneously with the 19.5-kHz transmitted pulse. Thus the count displayed on the time-interval meter was proportional to the range from the ship to the buoy. The count was also recorded on paper tape, along with the ping number, on a digital printing recorder. The ping number was necessary for correlating the recorded values of range with the data recorded on the Brush recorder and strip film camera.

CALIBRATION

The calibration system consisted of those components that were used in establishing the gain and operating levels of the two data receiving channels as well as establishing and measuring the power driving the transducer during the transmitted pulse. For the

receiving systems the output of the master 19.5-kHz crystal oscillator went to a voltage divider potentiometer that was used for accurately establishing a 1-volt signal for calibration purposes. The setting of the voltage divider was established and monitored by an ac vacuum-tube voltmeter. The 1-volt signal went into a precision attenuator, so that any level of calibrating signal could be accurately and readily selected. The output of that attenuator went to the calibrate positions of the calibrate-operate switches of the two receiving systems, thus enabling the substitution of accurately known calibration signals for received signals in the two receiving systems. For measuring the drive into the transducer during the transmitted pulse, an ac vacuum-tube voltmeter was used in conjunction with a cathode-ray oscilloscope. The input to the two instruments could be switched to either the input to the transmitter driver amplifier or across a low-resistance current shunt resistor in the transducer impedance-matching network, providing a direct measurement of transducer current. The voltmeter functioned primarily as a means for calibrating the oscilloscope, whereby a constant signal was used whose amplitude was adjusted to provide the same deflection on the scope as that of the pulses observed during transmission. The reading on the voltmeter was a measurement of the voltage across the current shunt resistor during the transmitted pulse and thus a measurement of transducer current.

SYSTEM PROGRAMMING

All timing functions of the complete instrumentation system were accomplished in the timing control unit. This unit provided the gating of the transmitted signal into the driver amplifier as well as the energization of the transmit-receiver transfer relay for transducer switching. Pulses from the unit were used for synchronizing the sweeps of the oscilloscopes displaying the received signals as well as triggering the camera control unit. For the buoy-range recording system the pulses of the unit's time base oscillator were used to drive the counters of the time interval meter, and the unit's reset generator was used for resetting the counters in the time interval meter. One of the variable delay pulses of the unit was used in the z-axis brightening of the monitor scope of the remote buoy system, providing the variable range mark.

TRANSDUCER POSITIONING

The transducer was positioned by a three-axis stablizied mount, so that any value of bearing and depression below the horizontal could be set for the acoustic beam axis. The settings could be readily made by handwheels and dials that electrically controlled electromechanical servo drive systems on the transducer mount. To maintain the beam axis in the same vertical plane as that containing the ship and buoy, a target-bearing transmitter, used for optically tracking the buoy, could be switched into the train drive system, substituting for the train control handwheel and dial, so that the transducer bearing was slaved to the optical bearing. To facilitate optical tracking of the buoy, smoke floats were dropped in close proximity to the buoy.

OTHER INSTRUMENTATION

In addition to the electronic instrumentation a dead-reckoning tracer was used for maintaining a record of the ship's maneuvers relative to geographic reference points as well as to the buoy location. For measuring the profile of vertical sound speed versus depth, a bathythermograph with a depth capability to 900 feet was used periodically. For maintaining a continuous record of the depth of the ocean, a precision depth recorder was employed in conjunction with an AN/UQN-1B sonar sounding set.

☆ U. S. GOVERNMENT PRINTING OFFICE : 1971—483-530/46

Security Classification

DOCUMENT CONTROL DATA - R & D

(Security classification of title, body of abstract and indexing annotation must be entered when the overall report is classified)

1. ORIGINATING ACTIVITY *(Corporate author)* Naval Research Laboratory Washington, D. C. 20390	2a. REPORT SECURITY CLASSIFICATION Unclassified 2b. GROUP

3. REPORT TITLE

BISTATIC ACOUSTIC SCATTERING FROM THE OCEAN BOTTOM

4. DESCRIPTIVE NOTES *(Type of report and inclusive dates)*

An interim report on continuing NRL Problems

5. AUTHOR(S) *(First name, middle initial, last name)*

B.G. Hurdle, K.D. Flowers, and K.P. Thompson

6. REPORT DATE August 5, 1971	7a. TOTAL NO. OF PAGES 22	7b. NO. OF REFS 12
8a. CONTRACT OR GRANT NO. NRL Problems S01-12 and S01-40 b. PROJECT NO. RF 101-03-44-4059 c. RF 05-552-402-Task 4070 d. SF 101-03-15-8181	9a. ORIGINATOR'S REPORT NUMBER(S) NRL Report 7285 9b. OTHER REPORT NO(S) *(Any other numbers that may be assigned this report)*	

10. DISTRIBUTION STATEMENT

Approved for public release, distribution unlimited.

11. SUPPLEMENTARY NOTES	12. SPONSORING MILITARY ACTIVITY Department of the Navy; Office of Naval Research, Arlington, Va. 22217 and Naval Ship Systems Command, Washington, D. C. 20360

13. ABSTRACT

To obtain the intensity field of sound scattered from a relatively rough region of ocean bottom, pulsed 19.5-kHz transmissions were directed toward the bottom from a ship as it approached and passed a special radio sonobuoy. Sets of data were taken with the beam incident on the bottom at grazing angles between 30 and 90 degrees. Bottom scatter returns in the monostatic direction were received on the source transducer, while reception in other directions was made by the buoy. The source was a tiltable piston transducer with a beamwidth of approximately 8 degrees. The buoy hydrophone was omnidirectional in the horizontal plane with a rejection of surface-reflected signals in the vertical plane. The data were analyzed on the basis of an isotropic-scatter model, taking the velocity gradient into consideration. Polar plots were made of bottom scattering strength. These intensity fields have been obtained from areas east of Bermuda for two bottom types, mud-coral and ooze, in water depths of approximately 750 and 1250 fathoms respectively. The results were compared with geometric reflection and Lambert's scattering law and did not correspond with either or with a combination of both. The shape of the plots of the measured field, combined with data indicating significant acoustic penetration into the bottom and data on the quantity of energy penetrating, suggests that a significant contribution to the field is made by a transmission path through the bottom. Sediment attenuation data in this frequency range, however, are inconclusive as to whether a significant contribution by refraction paths through the bottom exists.

DD FORM 1 NOV 65 1473 (PAGE 1)

S/N 0101-807-6801

Security Classification

Security Classification

14. KEY WORDS	LINK A ROLE	LINK A WT	LINK B ROLE	LINK B WT	LINK C ROLE	LINK C WT
Acoustic refraction						
Acoustic scattering						
Underwater acoustics						
Underwater sound transmission						
Underwater sound reverberation						
Ocean bottom						

DD FORM 1 NOV 65 1473 (BACK)
(PAGE 2)

Security Classification